Research Article | Vol. 13, No. 1 / 1 Jan 2022 / Biomedical Optics Express 197
Biomedical Optics EXPRESS

Cytotoxicity analysis of oxazine 4-perchlorate fluorescence nerve potential clinical biomarker for guided surgery

SANDRA PAMPÍN-SUÁREZ,[1] JOSÉ LUIS ARCE-DIEGO,[1] OLGA TAPIA,[2] FLOR MARÍA PÉREZ-CAMPO,[3] JOSÉ CARLOS RODRÍGUEZ-REY,[3] AND FÉLIX FANJUL-VÉLEZ[1,*]

[1]*Biomedical Engineering Group, TEISA Department, University of Cantabria, Avenida de los Castros 46, 39005 Santander, Spain*
[2]*Nuclear Cell Biology Group, Marqués de Valdecilla Health Research Institute (IDIVAL), Avenida Cardenal Herrera Oria s/n, 39011 Santander, Spain*
[3]*Tissue Engineering Group, Molecular Biology Department, University of Cantabria, Avenida Cardenal Herrera Oria 2, 39011 Santander, Spain*
[*]*fanjulf@unican.es*

Abstract: Biological tissue discrimination is relevant in guided surgery. Nerve identification is critical to avoid potentially severe collateral damage. Fluorescence imaging by oxazine 4-perchlorate (O4P) has been recently proposed. In this work, the cytotoxicity of O4P on U87 human-derived glioma cells has been investigated as a function of concentration and operating room irradiation modes. A custom-built optical irradiation device was employed for controlled optical dosimetry. DNA damage and O4P intracellular localization was also investigated by immunofluorescence and confocal microscopy. The results show that concentration below 100 μM can be considered safe. These results contribute to the assessment of the feasibility of O4P as a nerve biomarker.

1. Introduction

Biomedical optical diagnosis can be implemented by intrinsic label-free techniques [1]. These techniques facilitate clinical translation, as no exogenous component needs to be administered to the patient, and most of them can be non-contact. They can be based on measuring coherence [2], spectral [3,4], polarization [5] or even depolarization [6] information, among others. The aim of any of these diagnostic techniques is usually to distinguish between healthy and pathological biological tissues. Healthy tissue type discrimination is also a relevant clinical problem. It is fundamental to avoid undesired collateral effects in the particular case of guided surgery [7–9]. Healthy tissue discrimination is more complex in general with label-free techniques, compared with pathological tissue discrimination. Techniques such as diffuse reflectance spectroscopy (DRS) have been successfully applied to this problem [10]. Healthy tissue discrimination by DRS has demonstrated some difficulties with some specific biological tissue types, such as nerve or skin [11–13]. Nervous tissues are particularly challenging. This is due to the potential significance for the patient of collateral damage on this tissue type. It is then critical to clearly discriminate nervous tissue from other soft tissues during guided surgery.

The discrimination of nervous tissue during guided surgery can be implemented by extrinsic substances administered to the patient. The use of fluorescence agents has demonstrated its applicability in guided surgery for tumoral tissue discrimination [14] or treatment monitorization [15]. Approved clinical fluorophores, such as indocyanine green (ICG) or Methylene Blue (MB), are intended for tumoral tissue discrimination. For the particular case of nervous tissue fluorophores of the oxazine family have been proposed [16]. Among them, oxazine 4-perchlorate

#447773 https://doi.org/10.1364/BOE.447773
Journal © 2022 Received 8 Nov 2021; accepted 8 Nov 2021; published 7 Dec 2021

Biomedical Optics EXPRESS

(O4P) has demonstrated specificity on in vivo rats [17]. It is therefore a potential candidate for nervous tissue discrimination in guided surgery, showing increased contrast on peripheral nerve tissue [17–19], and central and peripheral nerve tissue [16]. The specificity is proved to be associated to nervous glial cells, with no significant accumulation on neuronal cells. Apart from nerve specificity, cytotoxicity is crucial for potential clinical translation of this fluorophore. Although some previous results on mice show no apparent behavioral effects, there is a need of quantitative and systematic cytotoxicity analysis [19]. This quantitative study of cytotoxicity is essential for the potential clinical applicability of the fluorophore. Cytotoxicity must be also tested as a function of irradiation [20], as the fluorophore is photoactivated and photobleached during a routine imaging diagnostic procedure.

In this work we analyzed cytotoxicity of O4P on U87 human-derived glioma cells. U87 glioma cell line was chosen among nervous tissue cell lines as representative of central nervous system glia, where O4P is expected to accumulate. Glial cells are estimated to be much more affected by the fluorophore in a dose-dependent model. Non-glial or other non-nervous tissues are proven not to accumulate significant amounts of O4P, and as a consequence are much less prone to suffer from cytotoxicity. In the case of neuronal cells, experiments on in vivo rats have demonstrated no apparent impairment of motor function and sensory integrity during the 24 h post-injection [16]. This cell line is also widely used and presents reasonable cultivation characteristics. Cytotoxicity was tested by a colorimetric proliferation assay for different O4P concentrations. The analyses included the potential effect of photoactivation and photobleaching by different irradiation spectra. A custom irradiation setup was built to be able to irradiate Petri dishes and multiwell plates. Two different irradiation spectra were considered, wide band visible (white) and a narrower spectrum around 630 nm. The first situation resembles conventional visible illumination in the operating room, while the second imitates fluorescence diagnostic imaging of O4P, as it comprises the absorption maximum. Immunofluorescence assays were also carried out to evaluate potential DNA damage. A significant DNA damage may not directly lead to cell death, but could greatly affect cell viability. The subcellular distribution of O4P is also investigated. The results show the potential safe O4P concentrations, as a function of irradiation type. The analysis considers cell death and DNA damage.

2. Materials and methods

2.1. Cell culture and fluorophore

Human-derived glioma U87 cell line (ATCC HBT-14) was grown as monolayer in Dulbeccós modified Eaglés medium (DMEM) (Lonza; Walkersville, MD, USA), supplemented with 10% fetal bovine serum (FBS) (HyClone, Global Life Science; Pasching, Austria), penicillin (100 U/mL) and streptomycin (100 µg/mL) (Lonza; Verviers, Belgium). Cell cultures were maintained in standard environmental conditions for their growth, at 37°C and in humidified atmosphere with 5% CO_2.

Oxazine 4-perchlorate (O4P) was provided by BOC Sciences (Bocsci; NY, USA). A stock solution was prepared at a concentration of 15 mM in phosphate buffered saline (PBS), pH 7.4 (Gibco; ThermoFisher Inc.). O4P has an absorbance peak at 616 nm and an emission peak at 635 nm in this solvent [16].

2.2. Irradiation and Imaging system

A custom-built irradiation system was employed. The system was designed to irradiate 60 mm diameter Petri dishes and 96 multiwell plates with 6 different types of optical radiation. The system consists of a high-power white LED source with 200 nm spectral width (MWWHLP1; Thorlabs Inc., USA). The source is driven by an electronic control system that allows modulation. The driver controls the emission irradiance. Six irradiation modes can be selected by means of

Biomedical Optics EXPRESS

a filter wheel. In this work the irradiation modes corresponding to white light (no filter) and 630 nm (FF01-630/92-25; Semrock, USA) are used. The resulting radiation is uniformized by an optical system, composed by a diffuser and a collimating lens, to achieve a homogeneous exposure across the surface of the Petri dish or the multiwell. Figure 1(A) shows a schematic of the device. The measured spectra of the incident radiation, either with white light (Fig. 1(B)) or light filtered at 630 nm (Fig. 1(C)) is also included in Fig. 1.

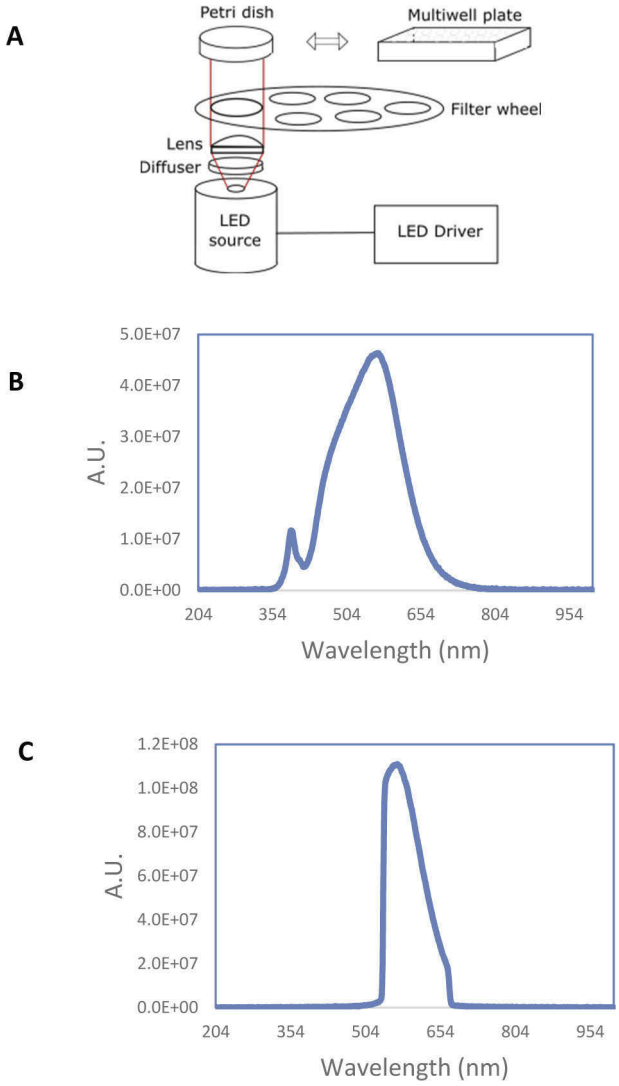

Fig. 1. A) Schematic design of the custom-made cell irradiation system, consisting of a driver-controlled broadband LED, a diffuser, a collimation system and a filter wheel for bandwidth selection. The system can irradiate Petri dishes and multiwell plates. B) White light irradiation spectrum. C) 630 nm irradiation spectrum.

Images of the cells were acquired using a Leica TCS SP5 inverted confocal microscope (Leica Biosystems; Wetzlar, Germany). O4P was excited using a laser at 633 nm. All images were analyzed using ImageJ software (NIH, Bethesda, Maryland, USA; http://rsb.info.nih.gov/ij/).

Biomedical Optics EXPRESS

2.3. Assay for cytotoxic activity

Viability of U87 cells was measured using CellTiter 96 AQueous One Solution Cell Proliferation Assay (PROMEGA; Madison, WI, USA), based on the MTS colorimetric assay [21]. MTS is a tetrazolium salt (3-(4,5-dimethylthiazol-2-yl)-5-(3-carboxymethoxyphenyl)-2-(4-sulfophenyl)-2H-tetrazolium) that turns into purple formazan in the presence of phenazine methosulfate, produced by NADPH-dependent dehydrogenases, which are active only in viable cells. Cells at a density of 104 cells/100 µL of culture media were inoculated in a 96-microwell plate (Corning; NY, USA).

After 24 h, cells were incubated with increasing concentrations of O4P (50, 100, 200, 400 µM) for 4 h. Light treatment was performed from below by means of the previously described custom-built irradiation device (Fig. 1). Cells were exposed to an irradiance of 10 mW/cm^2 for 15 min with both white light and at a wavelength $\lambda = 630$ nm. The wells were washed with PBS before being replaced with fresh culture. Cells were incubated overnight for 12 hours, and then O4P and irradiation cytotoxic effects were determined. To quantify the number of viable cells, 20 µL of CellTiter 96 AQueous One Solution Reagent was added following the manufacturer's instructions, and incubated for another 4 hours under the same conditions, after which the absorbance was measured at 490 nm.

The experiments were repeated 4 times. Cell viability was calculated according to the following equation: Cell viability (%) = (sample absorbance / control absorbance) x 100.

To evaluate the response of U87 cells to the different doses of O4P in the presence and absence of radiation, a two-way ANOVA analysis with several samples per group was carried out. Values with $p<0.05$ were considered statistically significant. Results were presented as relative mean ± standard deviation (SD) respect to control cells.

2.4. Immunofluorescence

Control, O4P treated and/or irradiated cells growing on polylysine-treated glass coverslips were used for immunofluorescence. Cells were fixed with 3.7% paraformaldehyde in PBS, washed in PBS and permeabilized with PBS which contained 0.5% Triton X-100. They were then incubated with 0.05% Tween 20 before adding the primary antibody (Mouse monoclonal anti-histone H2AX phosphoSer139, 1:200 immunostaining; Millipore-Upstate, MA, USA). Afterwards they were washed with PBS and treated with 0.05% Tween 20. Finally, they were incubated with the specific secondary mouse antibody conjugated with FITC (1:75 immunostaining; Jackson Laboratories Inc., USA). Samples were mounted with Vectashield (Vector; Burlingame, CA, USA). Fixed cells were stained with Propidium Iodide (PI), and DAPI to mark the nucleus.

Confocal images (1024 × 1024 pixels; 126.3 nm pixel size) were acquired on a SP5 laser-scan microscope (Leica Biosystems; Wetzlar, Germany), with a 40x/1.25 Oil objective, 2 Airy Units pinhole, 3x electronic zoom and 200 Hz speed using LAS AF acquisition software. Cells were excited at 405 nm (DAPI), 488 nm (ϒH2AX) and 543 nm (PI) laser lines and fluorescence emission was captured between 415-490 nm (DAPI), 500-550 nm (ϒH2AX) and 600-660 nm (PI). The choice of excitation sources and emission filters assures fluorophore specificity. Images are presented after digital adjustment of curve levels to maximize signal. In all cases, exposure time, sensor gain, and digital manipulation were the same for control and experimental samples. Fluorochromes and colours are as indicated in the corresponding figure legends.

The quantitative analysis of the proportion of control and U87 cells with DNA damage nuclear foci was carried out using ImageJ. The average of the fluorescence intensity was estimated on six confocal sections per sample ($n = 3$). Average values were pooled for the subsequent analysis using a two-way ANOVA with post-hoc Tukey HSD (Honestly Significant Difference) was used to determine the statistical significance of differences between control and irradiated cells. Values are mean values ± SD.

Biomedical Optics EXPRESS

2.5. Intracellular distribution of O4P

U87 cells were cultivated on polylysine-treated glass coverslips. Cells were treated with an appropriate amount of fluorophore for 4 hours. They were irradiated at 630 nm for 15 or 30 minutes, with the same conditions shown in the cytotoxicity assay. O4P was removed by washing twice with PBS buffer before their fixation with 3.7% paraformaldehyde in PBS. Cells were washed twice with PBS and were placed on a slide using an antifade mounting medium with DAPI (Vectashield, Vector; Burlingame, CA, USA).

Images of the cells were acquired using a Leica TCS SP5 inverted confocal microscope (Leica Biosystems; Wetzlar, Germany). DAPI was excited at 405 nm and radiation was collected between 415-490 nm, and O4P was excited using a laser at 633 nm and the emission was filtered in the range 645-700 nm. The composed images were obtained by ImageJ.

3. Results

The protocol described in materials and methods was applied to cell cultures with different fluorophore concentrations and irradiation types. As it can be seen in Fig. 2, dark controls do not exhibit statistically significant difference in cell death at the lowest non-zero concentration of fluorophore assayed (50 μM), compared with cells without treatment. However, the other amounts of O4P probed (100, 200 and 400 μM) produce significant decreases in cell viability of 12.92%, 63.09% and 93.81% respectively (Table 1).

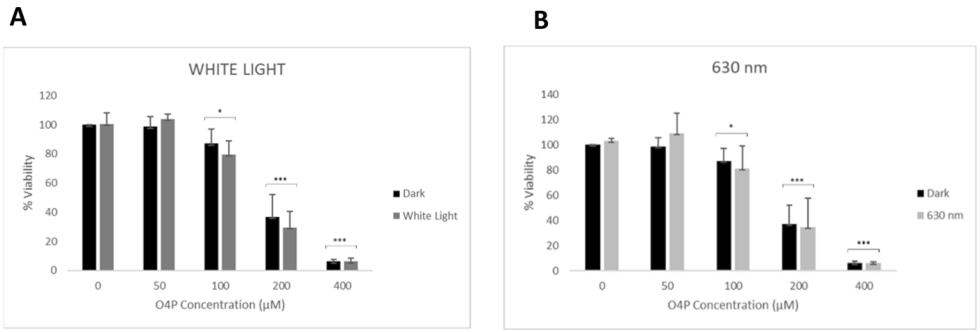

Fig. 2. Cytotoxicity assay results, expressed as percentage of viability of the U87 cells in dark and after 15 minutes of 10 mW/cm^2 irradiation with white light (A) and λ=630 nm light (B). Cells were treated with different amounts of O4P (0, 50, 100, 200 and 400 μM) for 4 h. These data represent the relative (in percentage) cell viability with respect to the negative control after 4 independent experiments. The results were analyzed using a two-factor ANOVA test with 6 samples per group. Statistical significance is indicated by *p<0.05, **p<0.01, ***p<0.001.

Table 1. Cytotoxic effect of the tested irradiations in combination with different concentrations of O4P on the percentage of cellular death in U87 cells. Results of 4 independent experiments expressed as relative Mean ± SD with respect to dark control.

	O4P concentration (μM)				
Light	0	50	100	200	400
Dark	100	98.72 ± 6.93	87.08 ± 10.23	36.91 ± 15.36	6.19 ± 1.41
White Light	100.49 ± 7.66	104.03 ± 3.21	79.61 ± 9.50	29.55 ± 10.94	6.13 ± 2.43
630 nm	103.04 ± 1.94	108.96 ± 16.00	81.18 ± 17.83	34.59 ± 23.23	5.94 ± 1.25

No statistical reduction in cell viability was detected with the irradiations tested. As it can be seen in Fig. 2(A), the combination of white light and the lowest dose (50 μM), does not induce

Biomedical Optics EXPRESS

changes in cell survival compared to cells with no fluorophore. However, as the concentration of O4P increases, a fall in the number of living cells takes place. At a concentration of 100 µM O4P, a decrease in cell viability around 15% was observed, which rises to 63% and 94% when the cells were incubated with 200 µM and 400 µM of compound, respectively (Table 1).

Figure 2(B) reflects the results obtained when cells were treated with red light at 630 nm wavelength, which corresponds to the fluorophore maximum absorption. A combination of 50 µM and 630 nm light practically produces no change in cell viability. This fact is in accordance to the previous cases of unirradiated controls and cells exposed to white light. On the other hand, growth inhibition was observed at 100, 200 and 400 µM O4P concentrations (18.82%, 65.41% and 94.06%, respectively). This impact on cell viability is comparable with that of dark and white light results (Table 1).

The IC50 calculated values are 169.87 µM, 184.79 µM and 142.65 µM for the dark controls, cells treated with white light and treated with red light at 630 nm, respectively. The IC50 of each group was estimated using an IC50 Calculator (https://www.aatbio.com/tools/ic50-calculator/).

Although at 630 nm the dose-response curve has shown a slight effect on cell growth, it can be assumed that the combination of O4P and the irradiation conditions assayed in this study had no effect on the viability of U87 cells.

Next, we investigate whether the presence of O4P may cause DNA damage in U87 cells, with or without light exposure. An immunofluorescence assay for the histone H2AX phosphorylated on Ser139 (ϒH2AX), a DNA damage marker, has been carried out and fluorescence intensity of DNA repair foci has been quantified (Figs. 3 and 4; ϒH2AX in green, PI in red, DAPI in blue). The aim is to mark nuclei (with DAPI), the whole cell (with PI) and the location of DNA damage in the nucleus (with ϒH2AX histone). The potential influence of O4P signal if it would be marginally contributing to the PI image in non-control samples, or the intensity of PI images are not relevant, as they are just employed to delineate cells and make images appear more realistic

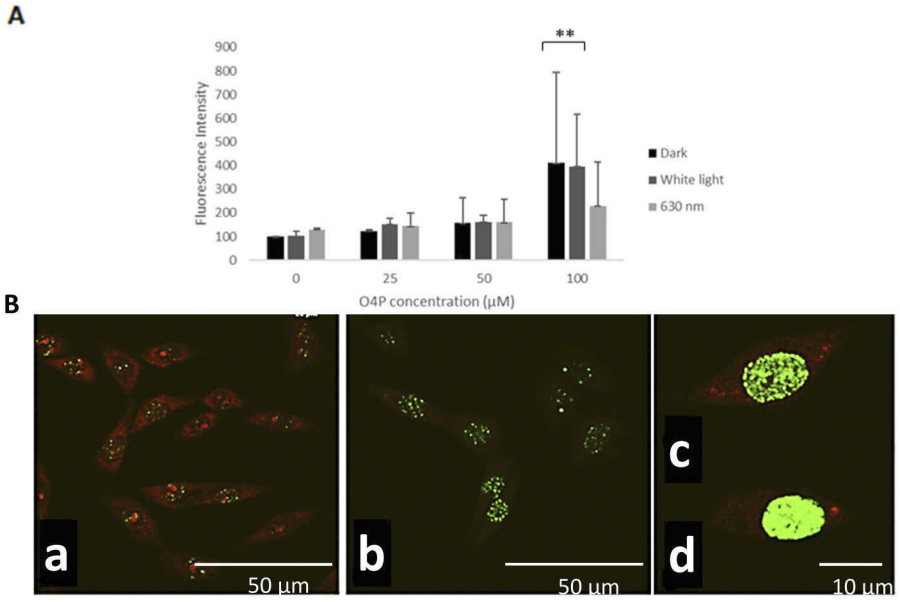

Fig. 3. DNA damage. A) Measurements of fluorescence intensity signals of ϒH2AX. B) High doses of O4P (100 uM) induce significant DNA damage (B.a), compared to control (B.b). In some of these cells, the amount of damage is dramatic (B.c, B.d). ϒH2AX (green), PI (red).

Biomedical Optics EXPRESS

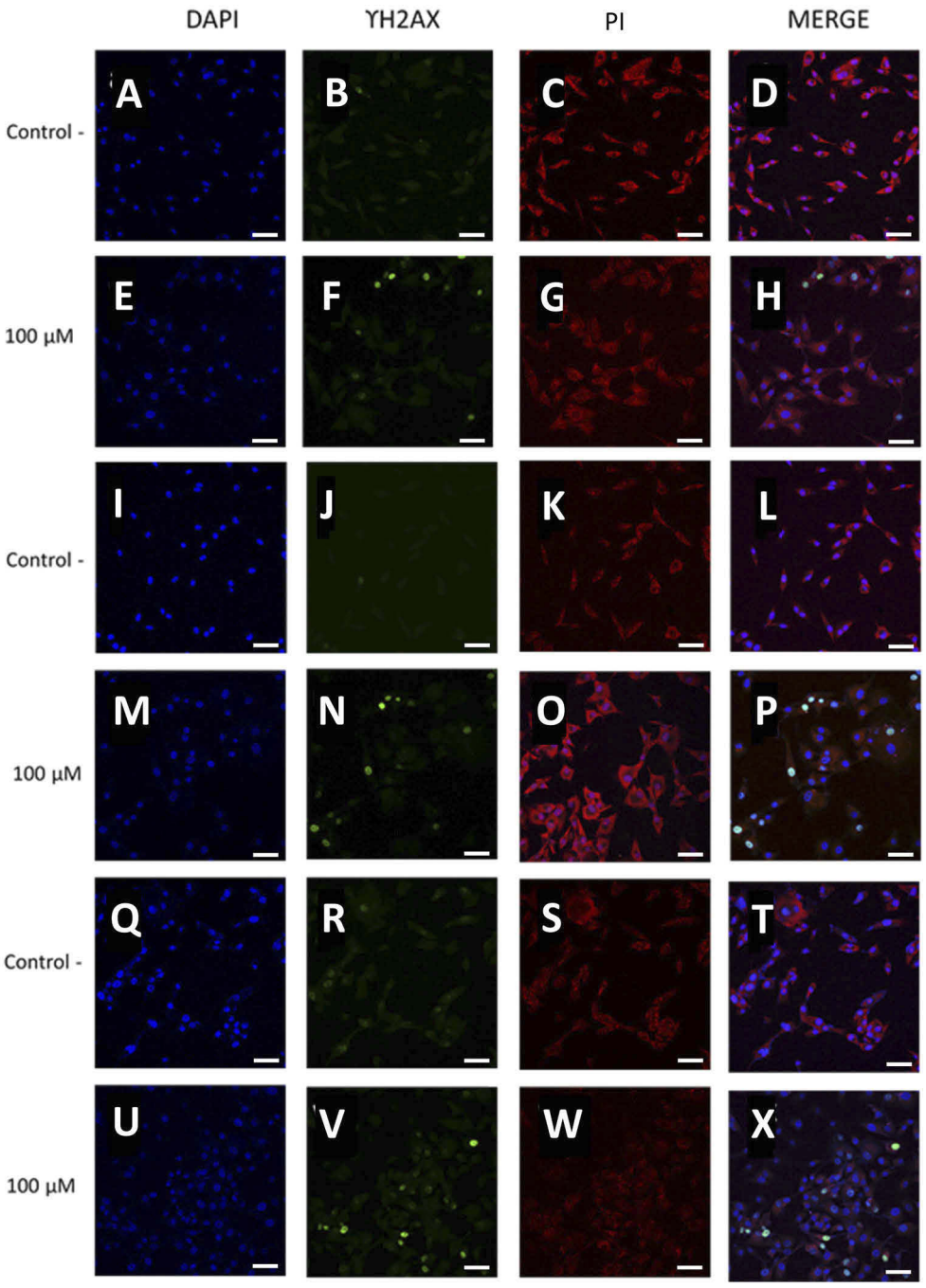

Fig. 4. Representative examples of confocal microscopy images from dark control (A–H), white light (I–P) or at 630 nm irradiated cells (Q-X). Comparison between cells in the absence of fluorophore (controls A-D, I-L and Q-T) and cells treated with 100 µM of O4P. DAPI (blue), ϒH2AX (green), and PI (red). Scale bar = 50 µm.

in the final merge. ϒH2AX test marks DNA damage, and it is intended to be a complementary analysis to further explore cell viability. Its utility is, on one side, to show cells that could be

Biomedical Optics EXPRESS

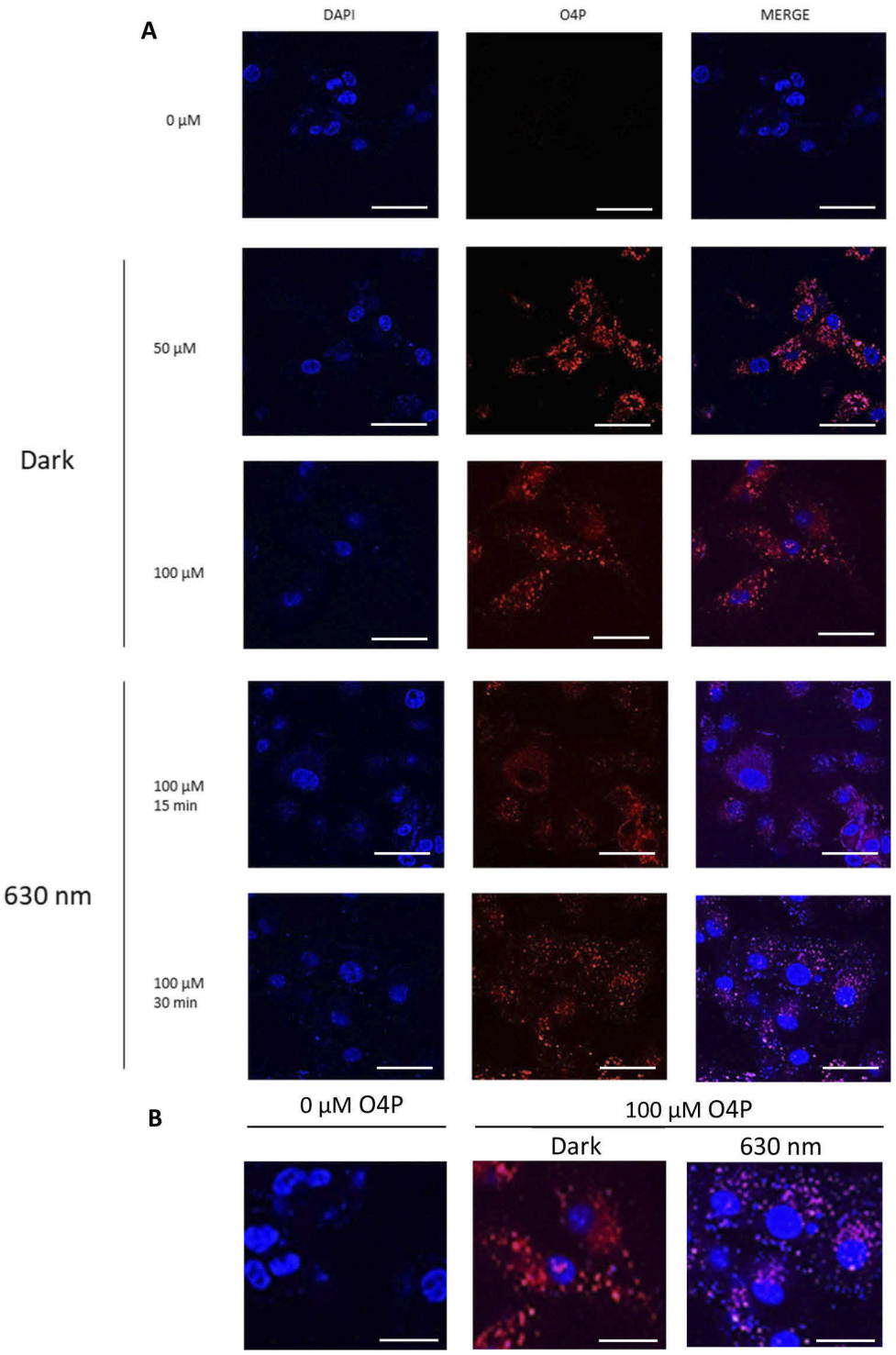

Fig. 5. O4P distribution (DAPI in blue, O4P in red). A) U87 confocal microscopy images treated with 50 and 100 µM of O4P either in dark or after irradiation at 630 nm for 15 and 30 min. Representative images of the localization of the fluorophore were taken after 4 hours of incubation. Nuclei labelled with DAPI are shown in blue. Scale bar = 25 µm. B) Higher magnification of merged images with no fluorophore and 100 µM. Scale bar = 20 µm.

Biomedical Optics EXPRESS

non-viable in the near future, even if they are marked as alive in the previous cell death test. On the other side, this analysis could help to refine the acceptable cytotoxic dose, that could be established under the IC50 cell death viability threshold if DNA damage is too high.

No significant differences have been observed between the lower fluorophore amounts tested (25 and 50 μM) and control (Fig. 3(A)). The signal for this active histone is notably increased, and appears concentrated in multiple nuclear foci, upon treatment with 100 μM of O4P (Fig. 3(B)). A qualitative analysis of the cells under a confocal microscope has shown that the cells exposed with the maximum concentration of O4P (100 μM) present a multitude of positive foci for H2AX in the nucleus compared with controls and cells treated with 25 and 50 μM O4P, although the number of positive cells is lower (Fig. 4).

Regarding the effect of irradiation with white light or at 630 nm, or combined with increasing concentrations of O4P, no significant differences have been observed between non-irradiated cells and those treated with light (Fig. 3).

The location of the fluorophore at the subcellular level was also investigated by confocal microscopy. U87 cells were grown with 0, 50 and 100 μM of O4P for 4 hours. Nuclei were marked with DAPI. Images obtained are shown in Fig. 5 (DAPI in blue, O4P in red). The control image of O4P (0 μM of O4P) appears black as expected, with no signal of DAPI. A uniform distribution of the molecule throughout the cytosol is observed, whereas it seems to be largely excluded from the nucleus.

To confirm if the light exposure causes any change in the subcellular location of the fluorophore, the experiment was repeated after irradiating at 630 nm for 15 and 30 minutes. As a consequence of photobleaching, a general intensity decrease with the radiation at 630 nm, compared to dark (no irradiation), is observed. As it can be seen in Fig. 5(A), irradiation did not alter the outcome. This effect is similar to the previous lack of influence of irradiation on cell viability. Irradiation does not modify O4P distribution under any of the conditions tested, being dispersed throughout the cytoplasm of the cell. Figure 5(B) shows higher magnification merged images that confirm the highly preferential accumulation of O4P in the cytoplasm.

4. Discussion

Accidental sectioning of peripheral or central nerves during common surgery interventions is relatively usual. However, there is currently no reliable technology available to discriminate nervous tissue from other ones in real time during surgical operations or laparoscopic procedures. Apart from the difficulty of developing highly specific fluorescent agents for nervous tissue per se, other inconvenient is that these molecules must be able to cross the blood-brain barrier (BBB) or the blood-nerve barrier (BNB). Therefore, they must have a small molecular size, around 500 Da as maximum, and a lipophilic character, with LogD values between 0.5 and 3 at pH 7.4. Oxazine 4 presents a molecular weight of 395.84 Da, with a LogD value at pH 7.4 of 3.38 [16]. As most compounds able to overcome these barriers are lipidic by nature, undesirable accumulation in the adjacent adipose tissue may appear [22,23].

Oxazine 4-perchlorate (O4P) is a small-sized fluorophore with high specificity for nervous tissue [17], which emits fluorescence at wavelengths close to the NIR window [16]. Due to its characteristics, it could be a good candidate for future applications in the field of medicine [18]. The success in clinical translation of O4P depends, in addition to its formulation and specificity, on its non-toxicity at the doses necessary to be detected. The safety of O4P was tested in this work by using a colorimetric assay to determine its toxicity on U87 cells treated with different concentrations of O4P (0, 50, 100, 100, 200 and 400 μM), see Fig. 2 and Table 1. These concentrations are considered to be representative of clinical use of O4P, as adequate nerve tissue contrast has been demonstrated with concentrations around 100 μM [16,17,19]. The obtained results indicate that this fluorescent compound affects the viability of this cell line in a dose-dependent manner. According to this study, it could be assumed that O4P concentrations

Biomedical Optics EXPRESS

lower than 100 µM are safe (considering the existence of toxic effect when there is less than 75% of cell viability). The theoretical half-maximum inhibitory concentration (IC50) was calculated to be 169.87 µM.

Since a main future objective is the use of the fluorophore in the operating room, the cytotoxicity of O4P in combination with white light and light at 630 nm was analyzed. Irradiance was kept constant at 10 mW/cm^2 and irradiation time was 15 minutes for all wavelengths. The results showed that there is not a synergistic effect on cytotoxicity between concentration and irradiation, see Fig. 2. According to these results, O4P induces cell death in our cellular model in a dose-dependent manner. As in the absence of light, there was a decrease in cell number of approximately 20% at 100 µM, of 70% at 200 µM and of 95% at 400 µM. The IC50 for irradiated cells was also very similar to that calculated for cells not treated with light, 184.79 µM and 142.65 µM for cells irradiated with white light and at 630 nm, respectively. From these findings, it can be ruled out that there is no increased toxicity due to photoactivation of O4P.

H2AX has a role in the DNA damage response induced from diverse origins. This protein is phosphorylated on the serine 139 residue rapidly after exposure of cells to ionizing radiation [24,25]. Immunofluorescence with this DNA damage marker was performed on U87 cells treated with 25, 50 and 100 µM O4P, both in the dark and irradiated with white light and at 630 nm, see Fig. 3 and Table 2. After quantification of the positive foci for the activated histone, no differences were observed either at the lower concentrations (25 and 50 µM), or among the diverse irradiation conditions used. However, at the highest concentration (100 µM), besides of a slight statistically significant increase in genome damage, qualitative changes are shown. More cells with deep damage, near apoptosis, were perceived, see Fig. 4. This fact is consistent with the decrease in cell viability seen at this concentration, which was around 20%. The multitude of positive foci at 100 µM compared to cells treated with 25 and 50 µM would explain the large standard deviations observed for the maximum concentration (Fig. 3(A) and Table 2).

Table 2. Total fluorescence intensity signal of ϒH2AX as a function of O4P concentration. Values of controls are normalized to 100% of fluorescence intensity. Values are mean ± SD versus control.

	O4P concentration (µM)			
Light	0	25	50	100
Dark	100	122.97 ± 7.05	156.84 ± 105.64	410.35 ± 382.80
White Light	101.69 ± 19.80	150.76 ± 26.63	162.26 ± 26.34	395.13 ± 221.28
630 nm	139.54 ± 5.62	143.52 ± 57.37	160.19 ± 96.00	228.43 ± 187.60

Intracellular localization of fluorophores can influence the molecular mechanism of cytotoxicity, impacting the cell and the quality of the signal during in vivo imaging [26,27]. As no significant nucleus colocalization was observed for O4P, with no change with photoexcitation, see Fig. 5, the distribution is estimated to be cytosolic. The cytosolic distribution of O4P suggests that the mechanisms involved in its toxicity are cytoplasmic, probably located in the mitochondria.

5. Conclusions

Guided surgery relies on an adequate identification of the biological tissues to be resected in real time. Apart from identifying malignant tumoral tissues, it is critical to clearly mark crucial tissues whose damage could provoke several collateral harmful effects. One of these critical tissues is nerve. Nerve identification is not solved, although there are some approaches based on fluorophores such as O4P. In this work the cytotoxicity of O4P on U87 human-derived glioma cells has been investigated. The analysis included the influence of irradiation type that could be present in the operating room, mainly wide band visible and that employed for fluorescence imaging of O4P around 630 nm. DNA damage was also investigated by immunofluorescence, in order to see if subtle potential harmful effects were being produced. O4P intracellular localization was

Biomedical Optics EXPRESS

also studied. The results show that there is a significant influence of fluorophore concentration, as expected. The influence of irradiation type, either white or around 630 nm, is negligible. Concentration values below 100 µM can be considered safe according to this study on glioma cells, including the effects of cell death and DNA damage. This study demonstrates the feasibility of employing O4P as a nerve marker under the point of view of cytotoxicity on human-derived glioma cells. Further studies should verify if the previously mentioned concentrations show no adverse effects on normal central and peripheral nerves, in vivo on small animals, and if they are able to provide enough image quality for nerve identification in the operating room. Although they are expected to suffer a reduced uptake, potential O4P cytotoxicity on other non-nervous tissue types should be also tested prior to clinical use.

Funding. Spanish Ministry of Science, Research and Universities, cofunded by FEDER funds (PGC2018-101464-B-I00); San Cándido Foundation.

Acknowledgments. The authors would like to acknowledge Drs. María Teresa Berciano and Miguel Ángel Lafarga for their useful comments and suggestions. Grant PGC2018-101464-B-I00, cofunded by FEDER funds, is entitled "High-pressure driven plasmonic and luminescence properties of naked and core/shell metal-oxide nanocomposites".

Disclosures. The authors declare no conflicts of interest.

Data availability. Data underlying the results presented in this paper are not publicly available at this time but may be obtained from the authors upon reasonable request.

References

1. V. V. Tuchin, *Tissue Optics: Light Scattering Methods and Instruments for Medical Diagnosis* (Society of Photo-Optical Instrumentation Engineers, 2015).
2. M. Villiger, D. Lorenser, R. A. McLaughlin, B. C. Quirk, R. W. Kirk, B. E. Bouma, and D. D. Sampson, "Deep tissue volume imaging of birefringence through fibre-optic needle probes for the delineation of breast tumour," Sci Rep **6**(1), 28771 (2016).
3. G. Bale, S. Mitra, J. Meek, N. Robertson, and I. Tachtsidis, "A new broadband near-infrared spectroscopy system for in-vivo measurements of cerebral cytochrome-c-oxidase changes in neonatal brain injury," Biomed. Opt. Express **5**(10), 3450–3466 (2014).
4. Q. Cao, N. G. Zhegalova, S. T. Wang, W. J. Akers, and M. Y. Berezin, "Multispectral imaging in the extended near-infrared window based on endogenous chromophores," J. Biomed. Opt **18**(10), 101318 (2013).
5. F. Fanjul-Vélez, M. Pircher, B. Baumann, E. Götzinger, C. K. Hitzenberger, and J. L. Arce-Diego, "Polarimetric analysis of the human cornea measured by polarization-sensitive optical coherence tomography," J. Biomed. Opt **15**(5), 056004 (2010).
6. N. Ortega-Quijano, F. Fanjul-Vélez, J. de Cos-Pérez, and J. L. Arce-Diego, "Analysis of the depolarizing properties of normal and adenomatous polyps in colon mucosa for the early diagnosis of precancerous lesions," Opt. Commun. **284**(19), 4852–4856 (2011).
7. A. V. DSouza, H. Lin, E. R. Henderson, K. S. Samkoe, and B. W. Pogue, "Review of fluorescence guided surgery systems: identification of key performance capabilities beyond indocyanine green imaging," J. Biomed. Opt **21**(8), 080901 (2016).
8. M. Rohde, F. Mehari, F. Klämpfl, W. Adler, F.-W. Neukam, M. Schmidt, and F. Stelzle, "The differentiation of oral soft- and hard tissues using laser induced breakdown spectroscopy – a prospect for tissue specific laser surgery," J. Biophotonics **10**(10), 1250–1261 (2017).
9. F. Fanjul-Vélez, I. Salas-García, and J. L. Arce-Diego, "Analysis of laser surgery in non-melanoma skin cancer for optimal tissue removal," Laser Phys. **25**(2), 025606 (2015).
10. F. Stelzle, K. Tangermann-Gerk, W. Adler, A. Zam, M. Schmidt, A. Douplik, and E. Nkenke, "Diffuse reflectance spectroscopy for optical soft tissue differentiation as remote feedback control for tissue-specific laser surgery," Lasers Surg. Med. **42**(4), 319–325 (2010).
11. G. C. Langhout, T. M. Bydlon, M. van der Voort, M. Müller, J. Kortsmit, G. Lucassen, A. J. R. Balthasar, G.-J. van Geffen, T. Steinfeldt, H. J. C. M. Sterenborg, B. H. W. Hendriks, and T. J. M. Ruers, "Nerve detection using optical spectroscopy, an evaluation in four different models: In human and swine, in-vivo, and post mortem," Lasers Surg. Med. **50**(3), 253–261 (2018).
12. F. Fanjul-Vélez, L. Arévalo-Díaz, and J. L. Arce-Diego, "Intra-class variability in diffuse reflectance spectroscopy: application to porcine adipose tissue," Biomed. Opt. Express **9**(5), 2297–2303 (2018).
13. F. Fanjul-Vélez, S. Pampín-Suárez, and J. L. Arce-Diego, "Application of classification algorithms to diffuse reflectance spectroscopy measurements for ex vivo characterization of biological tissues," Entropy **22**(7), 736 (2020).
14. I. Georgakoudi, B. C. Jacobson, J. Van Dam, V. Backman, M. B. Wallace, M. G. Müller, Q. Zhang, K. Badizadegan, D. Sun, G. A. Thomas, L. T. Perelman, and M. S. Feld, "Fluorescence, reflectance, and light-scattering spectroscopy for evaluating dysplasia in patients with Barrett's esophagus," Gastroenterology **120**(7), 1620–1629 (2001).

Biomedical Optics EXPRESS

15. I. Salas-García, F. Fanjul-Vélez, and J. L. Arce-Diego, "Superficial radially resolved fluorescence and 3D photochemical time-dependent model for photodynamic therapy," Opt. Lett. **39**(7), 1845–1848 (2014).
16. M. H. Park, H. Hyun, Y. Ashitate, H. Wada, G. Park, J. H. Lee, C. Njiojob, M. Henary, J. V. Frangioni, and H. S. Choi, "Prototype Nerve-Specific Near-Infrared Fluorophores," Theranostics **4**(8), 823–833 (2014).
17. C. W. Barth and S. L. Gibbs, "Visualizing oxazine 4 nerve-specific fluorescence ex vivo in frozen tissue sections," in *Molecular-Guided Surgery: Molecules, Devices, and Applications II* (International Society for Optics and Photonics, 2016), **9696**, p. 96960R.
18. F. Fanjul-Vélez, A. M. Díaz-Martínez, E. Garro-Martínez, and J. L. Arce-Diego, "Fluorescence imaging contrast in guided surgery on nerves measured in rats in vivo," in *Molecular-Guided Surgery: Molecules, Devices, and Applications VI* (International Society for Optics and Photonics, 2020), **11222**, p. 112220K.
19. L. G. Wang, C. W. Barth, C. H. Kitts, M. D. Mebrat, A. R. Montaño, B. J. House, M. E. McCoy, A. L. Antaris, S. N. Galvis, I. McDowall, J. M. Sorger, and S. L. Gibbs, "Near-infrared nerve-binding fluorophores for buried nerve tissue imaging," Sci. Transl. Med. 12(542), eaay0712 (2020).
20. S. L. Hopkins, B. Siewert, S. H. C. Askes, P. Veldhuizen, R. Zwier, M. Heger, and S. Bonnet, "An in vitro cell irradiation protocol for testing photopharmaceuticals and the effect of blue, green, and red light on human cancer cell lines," Photochem. Photobiol. Sci. **15**(5), 644–653 (2016).
21. T. L. Riss, R. A. Moravec, A. L. Niles, S. Duellman, H. A. Benink, T. J. Worzella, and L. Minor, "Cell viability assays," in *Assay Guidance Manual*, S. Markossian, A. Grossman, K. Brimacombe, M. Arkin, D. Auld, C. P. Austin, J. Baell, T. D. Y. Chung, N. P. Coussens, J. L. Dahlin, V. Devanarayan, T. L. Foley, M. Glicksman, M. D. Hall, J. V. Haas, S. R. J. Hoare, J. Inglese, P. W. Iversen, S. C. Kales, M. Lal-Nag, Z. Li, J. McGee, O. McManus, T. Riss, P. Saradjian, G. S. Sittampalam, M. Tarselli, O. J. Trask, Y. Wang, J. R. Weidner, M. J. Wildey, K. Wilson, M. Xia, and X. Xu, eds. (Eli Lilly & Company and the National Center for Advancing Translational Sciences, 2004).
22. X. Yuan and D. Taft, "Advanced formulation strategies for central nervous system drug delivery," in *Advanced Drug Formulation Design to Optimize Therapeutic Outcomes* (CRC Press, 2008).
23. S. L. Gibbs-Strauss, K. A. Nasr, K. M. Fish, O. Khullar, Y. Ashitate, T. M. Siclovan, B. F. Johnson, N. E. Barnhardt, C. A. T. Hehir, and J. V. Frangioni, "Nerve-highlighting fluorescent contrast agents for image-guided surgery," Mol. Imaging **10**(2), 7290.2010.00026 (2011).
24. E. P. Rogakou, D. R. Pilch, A. H. Orr, V. S. Ivanova, and W. M. Bonner, "DNA double-stranded breaks induce histone H2AX phosphorylation on serine 139 *," J. Biol. Chem. **273**(10), 5858–5868 (1998).
25. O. Fernandez-Capetillo, A. Lee, M. Nussenzweig, and A. Nussenzweig, "H2AX: the histone guardian of the genome," DNA Repair **3**(8-9), 959–967 (2004).
26. M. Redza-Dutordoir and D. A. Averill-Bates, "Activation of apoptosis signalling pathways by reactive oxygen species," Biochimica et Biophysica Acta (BBA) - Molecular Cell Research **1863**(12), 2977–2992 (2016).
27. J. V. Frangioni, "In vivo near-infrared fluorescence imaging," Current Opinion in Chemical Biology **7**(5), 626–634 (2003).